

Yb₂Pt₂Pb: Magnetic frustration in the Shastry-Sutherland lattice

M. S. Kim,^{1,2} M. C. Bennett,^{2,3} and M. C. Aronson^{1,2,3}

¹*Condensed Matter Physics and Materials Science Department,
Brookhaven National Laboratory, Upton, New York 11973-5000*

²*Department of Physics, University of Michigan, Ann Arbor, Michigan 48109-1120*

³*Department of Physics and Astronomy, Stony Brook University, Stony Brook, New York 11794-3800*

(Dated: November 2, 2018)

We have synthesized single crystals of Yb₂Pt₂Pb, which crystallize in the layered U₂Pt₂Sn-type structure, where planes of Yb ions lie on a triangular network. We report here the first results of magnetization, specific heat, and electrical resistivity experiments. The lattice constants and high temperature magnetic susceptibility indicate that the Yb ions are trivalent, while Schottky peaks in the specific heat show that the ground state is a well isolated doublet. Significant magnetic anisotropy is observed, with the ratio of susceptibilities perpendicular and parallel to the magnetic planes differing by as much as a factor of 30 at the lowest temperatures. Antiferromagnetic order occurs at a Néel temperature $T_N=2.07$ K, a transition temperature which is more than an order of magnitude smaller than the mean field interactions reflected by the in-plane Weiss temperature. Further evidence for short ranged magnetic fluctuations is found in the magnetic susceptibility and electrical resistivity, which have broad peaks above T_N , and in the slow development of the magnetic entropy at T_N . Our experiments indicate that Yb₂Pt₂Pb is a quasi-two dimensional and localized moment system, where strong magnetic frustration may arise from the geometry of the underlying Shastry-Sutherland lattice.

PACS numbers: 71.20.Eh, 75.30.Gw, 75.50.Ee

I. INTRODUCTION

Recently, the series of ternary compounds with composition R₂T₂M (R=rare earths or actinides; T=transition metals; M=Cd, In, Sn, and Pb) has attracted much attention because of the diversity of its collective phenomena, including ferromagnetic Kondo lattice,[1] Kondo semiconductor,[2] valence fluctuation,[3, 4, 5, 7] non-Fermi liquid,[6, 7] and heavy fermion ground states.[7, 8, 9]

Most of this series crystallize in the tetragonal Mo₂FeB₂-type structure (space group $P4/mbm$), which is an ordered derivative of the U₃Si₂-type. A smaller number of compounds crystallize in a distorted variant of this structure, the U₂Pt₂Sn-type structure (space group $P4_2/mnm$), which is a superstructure of the U₃Si₂-type.[10, 11, 12, 13, 14, 15] Both structures are intrinsically layered, with two types of layers which are alternately stacked along the c axis. The first layer type contains only R atoms, while the second layer type contains only T and M atoms. In the first layer type, the R atoms are arranged in a triangular motif, giving each R atom a single nearest neighbor. This structure is suggestive that planes of magnetic dimers may be formed, a necessary ingredient for novel spin liquid states, where frustration competes with order.

The crystal structure of the rare earth sublattices in both the Mo₂FeB₂ and U₂Pt₂Sn-types suggest that they may be rare examples of the two dimensional Shastry-Sutherland lattice, which has received substantial theoretical attention due to its exact dimerization and its spin liquid ground state.[23, 26] Currently, there are only a few known materials known to be examples of Shastry-

Sutherland systems. One such system is SrCu₂(BO₃)₂, which has a layered structure where each Cu²⁺ ion is antiferromagnetically coupled to a single nearest neighbor and to four next nearest neighbors, with each unit cell containing two of these dimers, which are mutually orthogonal. Features of this dimerized lattice include the absence of magnetic order, the formation of a spin gap at low temperature, and the appearance of plateaux in the magnetization with 1/4, 1/8, and 1/10 of the full saturated moment,[24, 25] as different ordered states emerge from the initially frustrated spin liquid through the application of magnetic fields.[26] Recently, similar plateaux have also been found in the magnetization of single crystalline TmB₄ and ErB₄ which form in the same space group as the layered Mo₂FeB₂-type structure, with the rare earth atoms forming the Shastry-Sutherland network.[28, 29, 30, 31]. Given this relationship between the Shastry-Sutherland lattice and the Mo₂FeB₂, U₂Pt₂Sn, and related crystal structure types, it is important to identify additional examples with different moment degeneracy and enhanced degrees of two-dimensionality.

It is known that a number of different members of the R₂T₂M series with R=Ce, Yb, or U form in either the Mo₂FeB₂ or U₂Pt₂Sn structures. In order to ascertain their suitability as exemplars of the Shastry-Sutherland lattice, it is important to establish whether the fundamental attributes of magnetic anisotropy, dimerization, and geometrical frustration are present. So far, most studies on these latter compounds have been conducted on polycrystalline samples, precluding a definitive answer to this question. We have recently succeeded in synthesizing single crystals of Yb₂Pt₂Pb, which crystal-

TABLE I: Results of the crystal structure refinement for $\text{Yb}_2\text{Pt}_2\text{Pb}$.

Space group	$P4_2/mnm$ (No. 136)
Lattice parameters	$a = 7.7651(6) \text{ \AA}$ $c = 7.0207(7) \text{ \AA}$
Formula units per cell	$Z = 4$
Cell volume	423.327 \AA^3
Calculated density	14.80 g/cm^3
Conventional Rietveld reliability factors ^a :	
$R_P = 0.0976$, $R_{WP} = 0.1290$, $R_{\text{exp}} = 0.1145$	
$R_B = 0.0361$, $R_F = 0.0265$	
Goodness of fit	$\chi^2 = 1.28$

^a R_P : Profile factor, R_{WP} : Weighted profile factor, R_{exp} : Expected weighted profile factor, R_B : Bragg factor, R_F : Crystallographic factor

TABLE II: Crystallographic data for $\text{Yb}_2\text{Pt}_2\text{Pb}$ at room temperature.

Wyckoff		x	y	z	$U_{\text{eq}}^a(\text{\AA}^2)$
Yb1	$4f$	0.1771(8)	x	0	0.0074(23)
Yb2	$4g$	0.3386(8)	$-x$	0	0.0055(21)
Pt	$8j$	0.3730(3)	x	0.2747(9)	0.0066(9)
Pb	$4d$	0	1/2	1/4	0.0050(9)

^a U_{eq} stands for the isotropic thermal parameter defined as one-third of the trace of the orthogonalized U_{ij} tensor.

lize in the tetragonal $\text{U}_2\text{Pt}_2\text{Sn}$ -type structure.[15] Here, we present a first report of the anisotropic magnetization and magnetic susceptibility, the specific heat, and the electrical resistivity. We will argue here that the Yb moments in $\text{Yb}_2\text{Pt}_2\text{Pb}$ lie on a lattice which is equivalent to the Shastry-Sutherland lattice.

II. EXPERIMENTAL DETAILS

Single crystals of $\text{Yb}_2\text{Pt}_2\text{Pb}$ were grown from a Pb flux, forming in a rod-like morphology with a square cross-section. Elements in the ration $\text{Yb}:\text{Pt}:\text{Pb} = 5:4:40$ were placed in an alumina crucible and then sealed in an evacuated quartz tube. The materials were initially held at $1180 \text{ }^\circ\text{C}$ for four hours, and subsequently cooled to $450 \text{ }^\circ\text{C}$ at $7 \text{ }^\circ\text{C}$ per hour. Excess Pb was removed by centrifuging the tubes at $450 \text{ }^\circ\text{C}$. Laue photo images indicate that the crystallographic c axis ($[001]$) lies along the long axis of the crystal, while the a ($[100]$) and b ($[010]$) axes define the square cross-section of the rod. Electron-probe microanalysis was carried out on polished single crystals using a Cameca SX100 microprobe system with elemental Yb, Pt, and Pb standards. The atomic ratio of $\text{Yb}:\text{Pt}:\text{Pb}$ is found to be $40.5 \pm 0.3\% : 39.2 \pm 0.4\% : 20.2 \pm 0.5\%$, and is spatially uniform over the whole crystal surface. X-ray diffraction was performed on a powder prepared from the single crystals. The diffraction patterns were

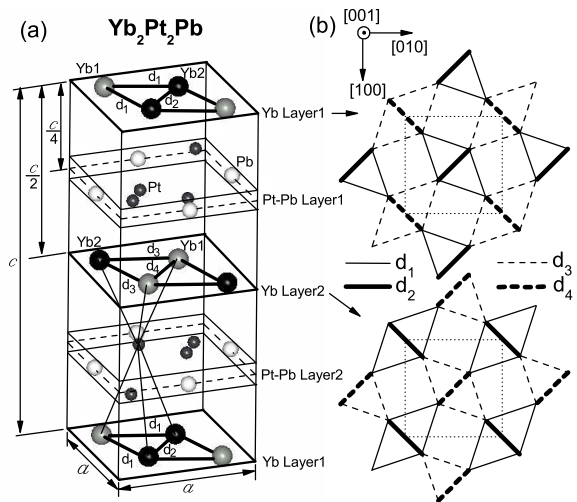


FIG. 1: (a) Schematic representation of the unit cell of $\text{Yb}_2\text{Pt}_2\text{Pb}$ crystallizing in the tetragonal $P4_2/mnm$ (No. 136) structure. (b) Lattice structure of the Yb ions in Yb layer 1 (top) and 2 (bottom). The Yb ions lie at the vertices of the triangles and the dotted lines delineate the unit cell.

refined using Fullprof. Refinement results and crystallographical data are listed in Tables I and II, respectively. Both confirm that $\text{Yb}_2\text{Pt}_2\text{Pb}$ has the previously reported $\text{U}_2\text{Pt}_2\text{Sn}$ -type structure.[15]

Magnetic susceptibility measurements were performed using a Quantum Design Magnetic Property Measurement System (MPMS) and a Vibrating Sample Magnetometer (VSM) in a Quantum Design Physical Property Measurement System (PPMS) over temperature ranges of $1.8 \text{ K} < T < 300 \text{ K}$ and $300 \text{ K} < T < 800 \text{ K}$, respectively. Magnetization measurements were performed using the VSM in magnetic fields up to 14 T. The electrical resistivity was measured by the conventional four-probe method in the temperature range $0.4 < T < 300 \text{ K}$. Specific heat measurements were carried out for temperatures between 0.4 K and 100 K.

III. CRYSTAL STRUCTURE

In the tetragonal Mo_2FeB_2 -type structure, T and M atoms of $\text{R}_2\text{T}_2\text{M}$ lie in the same plane, while T atoms in the tetragonal $\text{U}_2\text{Pt}_2\text{Sn}$ -type structure are displaced out of the plane, as demonstrated in the crystal structure of $\text{Yb}_2\text{Pt}_2\text{Pb}$ shown in Fig. 1(a). Here, two of the four Pt atoms on the middle of the Pt-Pb plane are shifted down (up) and the other two close to the edge of the plane are shifted up (down) in the Pt-Pb layer 1 (in the Pt-Pb layer 2) without any shift of Pb atoms from the plane. These displacements result in two kinds of Yb-Pt tetrahedra, with large and small heights as shown in Fig. 1(a). The shifted Pt atoms force the Yb atoms to form two different

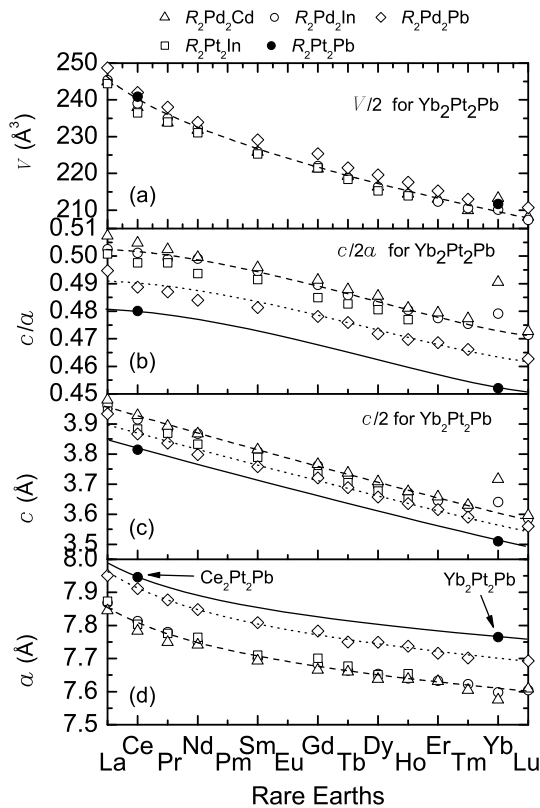


FIG. 2: Comparison of lattice parameters a and c , the ratio c/a , and the unit cell volume V for R_2T_2M (R =rare earths, T =Pd and Pt, M =Cd, In, and Pb).[4, 5, 15, 19, 20, 21] Solid, dotted, and dashed lines are guides for the eye.

networks of isosceles triangles ($d_1 = 3.9646 \text{ \AA}$ and $d_2 = 3.5451 \text{ \AA}$ in Yb layer 1, and $d_3 = 4.1960 \text{ \AA}$ and $d_4 = 3.8890 \text{ \AA}$ in Yb layer 2), leading to a superstructural distortion with a doubled lattice parameter c . Among the rare earth and actinide intermetallics, only a few display a similar superstructural distortion.[10, 11, 12, 13, 14, 15] On the other hand, in the Yb layer 1 and 2, Yb atoms are arranged in the network of mixed rectangles and isosceles triangles as shown in Fig. 1(b), implying that the two rare earth layers can separately be considered topologically similar to Shastry-Sutherland lattices.[23] This suggests that magnetic frustration is likely to be an important feature of the magnetic behavior in Yb_2Pt_2Pb .

Fig. 2 compares the structural parameters for some members of the R_2T_2M (R =rare earths; T =Pd and Pt; M =Cd, In, and Pb) series [4, 5, 15, 19, 20, 21] which crystallize in the tetragonal Mo_2FeB_2 -type structure, except for Yb_2Pt_2Pb which has the U_2Pt_2Sn -type structure. All parameters gradually decrease as the R atoms are changed from La to Lu, due to the lanthanide contraction. For comparison, $c/2$, $c/2a$, and $V/2$ are plotted for Yb_2Pt_2Pb . For lattice parameters a and c , we find the relation of $a(Pt, Pb) > a(Pd, Pb) > a(Pt, In) \gtrsim a(Pd, In) \gtrsim a(Pd, Cd)$

and $c(Pd, Cd) \gtrsim c(Pd, In) \gtrsim c(Pt, In) > c(Pd, Pb) > c(Pt, Pb)$. Considering atomic radii r ($r_{Pt} \gtrsim r_{Pd}$ and $r_{Pb} > r_{In} \gtrsim r_{Cd}$), this indicates that the increase of the sum of the radii of T and M atoms underlies the increase of the lattice parameter a and the decrease of the lattice parameter c . The inverse dependence of c compensates the dependence of a resulting in a much weaker variation in the unit cell volume with rare earth atom, as shown in Fig. 2(a). We note that the anomalously large values of c and c/a found in Yb_2Pd_2M (M =Cd and In) are caused by the intermediate valence of Yb in these compounds.[4, 5, 6, 7] In contrast, the values of c and c/a in Yb_2Pt_2Pb are consistent with those of other compounds with trivalent rare earth ions. This indicates that Yb in Yb_2Pt_2Pb is in a stable trivalent Yb state, without mixed valence character. From the unusually low value of c/a found in Yb_2Pt_2Pb , we anticipate strongly anisotropic behavior.

Among the R_2Pt_2Pb (R =rare earth) series, only Ce_2Pt_2Pb [21] and Yb_2Pt_2Pb have previously been reported. Note that Ce_2Pt_2Pb crystallizes in the tetragonal Mo_2FeB_2 -type structure, while Yb_2Pt_2Pb forms in the distorted U_2Pt_2Sn -type variant. One might thus expect that R_2Pt_2Pb compounds comprised of light rare earths R may crystallize in the tetragonal Mo_2FeB_2 -type structure, while the heavy rare earths crystallize in the tetragonal U_2Pt_2Sn -type structure. A similar effect was observed in the R_2Au_2In series,[14] where only the heavy rare earths R =Tm and Lu crystallize in the tetragonal U_2Pt_2Sn -type structure. Considering the lanthanide contraction, this indicates that the small size of the heavy rare earth atoms plays an important role in enabling the superstructural distortion. Specifically, we suggest that the displacement of the T atoms in R_2T_2M with the tetragonal U_2Pt_2Sn -type structure only occurs for small R atoms. This proposal is supported by the observations that the compounds with divalent Yb (Yb_2Cu_2In and Yb_2Au_2In) [17, 18] and the compounds with mixed valent Yb (Yb_2Pd_2Cd , Yb_2Pd_2In , and Yb_2Pd_2Sn),[4, 5, 6, 7] where the Yb atoms all have relatively large size, instead crystallize in the Mo_2FeB_2 -type structure and not in the U_2Pt_2Sn -type structure. Conversely, it seems that Yb atoms in the tetragonal Mo_2FeB_2 -type structure prefer divalent or mixed valent states to the trivalent state, while Yb atoms in the tetragonal U_2Pt_2Sn -type structure prefer trivalent states. We note that Yb_2Pt_2Pb is the only one of the reported Yb compounds of R_2T_2M series which is trivalent. Recently, composition dependent magnetic order has been found in compounds of the series $Yb_2Pd_2In_{1-x}Sn_x$ for $x = 0.6$ and 0.8 , intermediate between the mixed valent endpoints Yb_2Pd_2In and Yb_2Pd_2Sn . [6] Also, applying pressures between 1 and 4 GPa causes Yb_2Pd_2Sn to order magnetically.[22] These observations of magnetic order imply that the Yb ions are trivalent. It would follow, then, that the crystal structures of these compounds may well be distorted from the tetragonal Mo_2FeB_2 -type structure, possibly into the U_2Pt_2Sn -type structure found in Yb_2Pt_2Pb . It would be

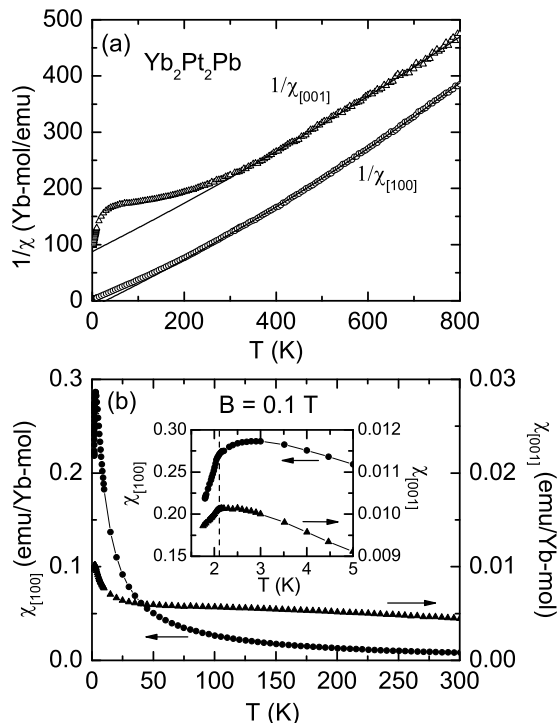


FIG. 3: (a) Temperature dependences of the inverse susceptibilities $1/\chi_{[100]}$ (○) and $1/\chi_{[001]}$ (Δ) up to 800 K. The magnetic susceptibility at $300 \text{ K} < T < 800 \text{ K}$ was measured in 2 T. The solid lines represent a fit with a modified Curie-Weiss law at $300 \text{ K} < T < 800 \text{ K}$ (see text) (b) Temperature dependence of magnetic susceptibilities $\chi_{[100]}$ (●) and $\chi_{[001]}$ (▲) for $B||[100]$ and $B||[001]$, respectively, below 300 K in 0.1 T. The inset shows an enlarged plot of $\chi_{[100]}$ and $\chi_{[001]}$ with $T < 5 \text{ K}$.

interesting to test for such a structural change in these magnetically ordering compounds.

IV. PHYSICAL PROPERTIES

A. Experimental results

Fig. 3(a) shows the inverse of the magnetic susceptibilities $1/\chi_{[100]}$ and $1/\chi_{[001]}$, measured with a magnetic field $B = 0.1 \text{ T}$ along [100] and [001], respectively, below 800 K. The data between 300 K and 800 K are well described by a modified Curie-Weiss law ($\chi = \chi_0 + C/(T - \theta)$), which gives $\chi_0 = -0.0006 \text{ emu/Yb-mol}$, a Weiss temperature $\theta_{[100]} = 28 \text{ K}$, and an effective moment $\mu_{\text{eff}} = 4.42 \mu_B$ for $1/\chi_{[100]}$, while $\chi_0 = -0.0004 \text{ emu/Yb-mol}$, $\theta_{[001]} = -217 \text{ K}$, and $\mu_{\text{eff}} = 4.54 \mu_B$ for $1/\chi_{[001]}$. The effective moments deduced from $1/\chi_{[100]}$ and $1/\chi_{[001]}$ are very close to $4.54 \mu_B$, as expected for free Yb^{3+} ions. This indicates that the Yb moments in $\text{Yb}_2\text{Pt}_2\text{Pb}$ are well localized and trivalent at high temperatures, consistent with the analysis of the crystal structure.

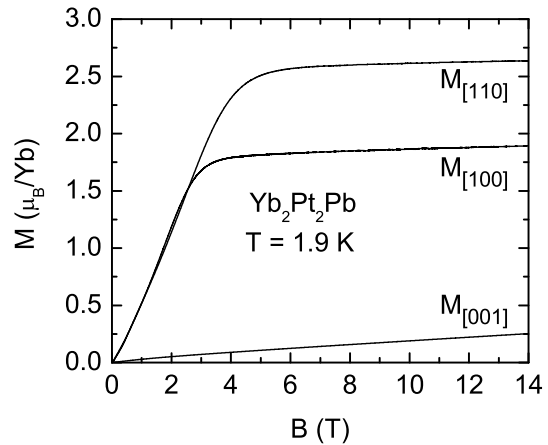


FIG. 4: (a) Magnetic field dependences of the magnetizations $M_{[001]}$, $M_{[100]}$, and $M_{[110]}$ for $B||[001]$, $B||[100]$, and $B||[110]$, respectively.

Fig. 3(a) shows that both $1/\chi_{[100]}$ and $1/\chi_{[001]}$ increasingly deviate from Curie-Weiss behavior below 300 K, and that this deviation is particularly marked for $1/\chi_{[001]}$. As indicated in Fig. 3(b), $\chi_{[001]}$ is nearly independent of temperature down to 30 K, with magnitude of only $\sim 5 \times 10^{-3} \text{ emu/Yb-mol}$, displaying a residual tail at the lowest temperatures. For $1/\chi_{[100]}$, the deviation from the Curie-Weiss law is less pronounced, and is only detected below 150 K. The inset of Fig. 3(b) shows $\chi_{[100]}$ and $\chi_{[001]}$ below 5 K. A broad maximum is found for $\chi_{[100]}$ and especially $\chi_{[100]}$ between 2-3 K, while a sharp cusp-like anomaly is found in $\chi_{[001]}$ and a weaker anomaly in $\chi_{[100]}$, indicating the onset of magnetic order at 2.07 K.

The magnetic susceptibility is strongly anisotropic, with $\chi_{[100]}/\chi_{[001]} \sim 30$ at low temperatures, a value which is even larger than that found in $\text{R}_2\text{Cu}_2\text{In}$ ($\text{R}=\text{Gd-Tm}$). [16] Fig. 4(a) shows the field dependence of the magnetizations $M_{[110]}$, $M_{[100]}$, and $M_{[001]}$, measured at 1.9 K with the magnetic field oriented along the different principal directions, [110], [100], and [001]. It is clear that the magnetic hard axis is along [001], since here $M_{[001]}$ reaches only $0.25 \mu_B/\text{Yb}$ in fields as large as 14 T. In contrast, $M_{[110]}$ and $M_{[100]}$ gradually increase and then saturate at $2.6 \mu_B$ and $1.9 \mu_B$ above 5 T and 3 T, respectively. This last observation indicates that the [110] is the easy direction in the plane, while the limited anisotropy between the [110] and [100] directions shows that this anisotropy is very small compared to the anisotropy which confines the moments to the layers themselves.

The inset of Fig. 5(a) shows the temperature dependence of the electrical resistivity ρ with the current flowing along [001]. The resistivity is definitively metallic, gradually decreasing with a weak positive curvature from its initial value of $26 \mu\Omega\text{cm}$ at 300 K. The resistivity of

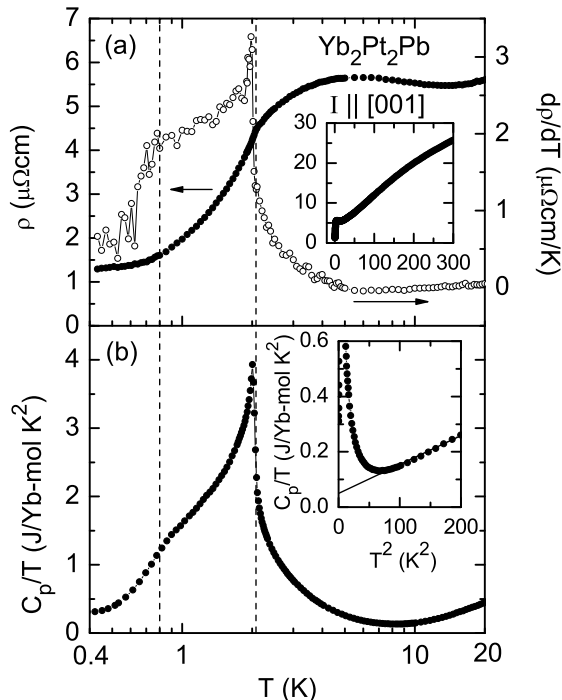


FIG. 5: (a) Logarithmic temperature dependence of the resistivity ρ (●) and the temperature derivative of the resistivity $d\rho/dT$ (○) below 20 K. The inset shows the temperature dependence of ρ over an expanded temperature range. (b) Logarithmic temperature dependence of the specific heat divided by temperature C_p/T below 20 K. The inset shows the plot of C_p/T vs T at high temperatures. Solid line in the inset indicates the fit of $C_p/T = \gamma_h + \beta T^2$ above 8 K.

most polycrystalline compounds from the R_2T_2M series is very high, typically several hundreds of $\mu\Omega\text{cm}$ at 300 K and several tens of $\mu\Omega\text{cm}$ even at the lowest temperatures. For $\text{Yb}_2\text{Pt}_2\text{Pb}$, the much lower resistivity at 300 K indicates very good crystal quality and a near optimal growth of our single crystals. Fig. 5(a) shows that with decreasing temperature, a shallow minimum is found in ρ at 13 K, followed by a broad maximum preceding the sudden drop at 2.07 K, the same temperature at which magnetic order is detected in $\chi_{[100]}$ and $\chi_{[001]}$. Additional evidence for magnetic order is found in the specific heat divided by temperature C_p/T , where a sharp peak is found at 2 K, as shown in Fig. 5(b). Remarkably, Fig. 5(b) demonstrates that the temperature dependences of C_p/T and $d\rho/dT$ are virtually identical, both above and below the 2.07 K ordering temperature. Both show distinct shoulder-like anomalies near 0.8 K, terminating at the lowest temperatures in a residual resistivity $\rho_0 = 1.3 \mu\Omega\text{cm}$ and an electronic part of the specific heat $\gamma = 311 \text{ mJ/Yb-molK}^2$, respectively. Given the high quality of our crystals, we believe that the shoulder-like feature is intrinsic to $\text{Yb}_2\text{Pt}_2\text{Pb}$ and does not result from the inclusion of a secondary phase. However, it proves

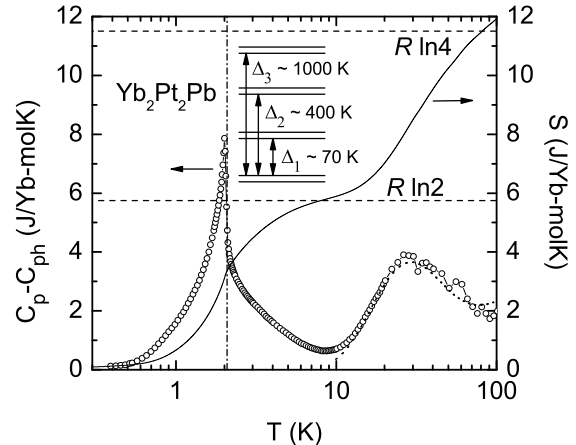


FIG. 6: The temperature dependence of the measured specific heat C_p from which we have subtracted an estimated phonon contribution C_{ph} , and the associated entropy S . The dotted line represents a fit to a Schottky expression. The schematic diagram of the CEF levels from the fitting is presented in the inset.

impossible to fit these data over a convincing range of temperatures using any of the conventional expressions for spin waves, either with or without gaps.

Fig. 6 shows the magnetic contribution of the specific heat $C_p - C_{\text{ph}}$, which is obtained by subtracting C_{ph} , the phonon contribution of the specific heat estimated from the Debye model from the measured specific heat, C_p . The Debye temperature, $\theta_D = 184 \text{ K}$ is obtained by fitting $C_p/T = \gamma_h + \beta T^2$ above 8 K, as shown in the inset of Fig. 5(b). The entropy S is only $0.58R \ln 2$ at 2.07 K. With increasing temperature, $C_p - C_{\text{ph}}$ shows a long tail up to 8 K at which a minimum is found and where the entropy S recovers its full value of $R \ln 2$. The long tail between 2.07 K and 8 K is consistent with the broad maxima in $\chi_{[100]}$ and ρ along $[001]$ in indicating the presence of short ranged magnetic fluctuations in this temperature range. The entropy S remains approximately constant between 10 and 15 K, indicating that magnetic order develops from a well-separated doublet ground state. A broad maximum is found near 30 K in $C_p - C_{\text{ph}}$, which can be identified as a Schottky anomaly with an energy splitting scheme of $\Delta_1 \sim 70 \text{ K}$, $\Delta_2 \sim 400 \text{ K}$, and $\Delta_3 \sim 1000 \text{ K}$ between the four doublets expected for the crystalline electric field (CEF) induced by the local $m2m$ symmetry of Yb sites in $\text{Yb}_2\text{Pt}_2\text{Pb}$, as shown in the inset of Fig. 6. With increasing temperature, S gradually increases and eventually reaches $R \ln 4$ around 70 K, as expected, given the observation of the Schottky anomaly at 30 K. This scale of crystal field splittings is comparable to that found in inelastic neutron scattering measurements on $\text{Yb}_2\text{Pd}_2\text{In}$.^[6]

B. Discussion

Our analysis of crystal structure trends in isostructural rare earth compounds provides indirect evidence that the Yb moments in $\text{Yb}_2\text{Pt}_2\text{Pb}$ are trivalent. Magnetic susceptibility measurements confirm this result, finding a conventional paramagnetic state above ~ 300 K which involves fluctuations of the full Yb^{3+} moment. Specific heat measurements confirmed that the crystal electric field scheme is consistent with the local site symmetry for the Yb^{3+} moments. Further, these measurements indicate that the ground state of $\text{Yb}_2\text{Pt}_2\text{Pb}$ involves a well isolated doublet for the Yb moments.

Cusp-like anomalies in the magnetic susceptibilities $\chi_{[100]}$ and especially $\chi_{[001]}$ indicate the onset of antiferromagnetic order at 2.07 K. Given the layered crystal structure and the strong magnetic anisotropy which largely confine the Yb moments to these layers, we might have expected that intermoment interactions would be strong and antiferromagnetic in the plane, and weaker between moments in neighboring planes. In fact, the opposite situation is found. The Weiss temperature $\theta_{[001]} (= -217$ K), found when the field is perpendicular to the layers, is approximately an order of magnitude larger than the in-layer Weiss temperature $\theta_{[100]} (= 28$ K). We conclude, then, that the anisotropy conferred on the Yb moments by the crystal electric field must be the dominant factor in establishing magnetic anisotropy in $\text{Yb}_2\text{Pt}_2\text{Pb}$. In this way, the competition between the strong antiferromagnetic interactions between planes and the weaker ferromagnetic interaction within the planes results in a complex magnetic structure and its accompanying fluctuations. Consequently, a sharp lambda-like anomaly is found in the specific heat at 2.07 K, a temperature which is more than two orders of magnitude lower than the inter-plane interaction scale projected by the Weiss temperature $\theta_{[001]} = -217$ K, and one order of magnitude weaker than the ferromagnetic in-plane interactions implied by the Weiss temperature $\theta_{[100]} = 28$ K. The temperature dependences of the specific heat and the temperature derivative of the electrical resistivity are nearly identical, both above and below the magnetic transition. This implies that the resistivity is dominated by forward scattering, as expected in a system with an abundance of small wave-vector critical fluctuations, such as a ferromagnet.[34] We conclude that the magnetic structure of $\text{Yb}_2\text{Pt}_2\text{Pb}$ may be rather complex, with mixed antiferromagnetic and ferromagnetic character, perhaps reflecting the geometrically frustrated nature of the Shastry-Sutherland lattice. One possibility for the zero-field structure would be a long-wave ferromagnetic spiral, as has been proposed theoretically.[35, 36]

However, the underlying symmetries of the crystal lattice constrain the magnetic structure of $\text{Yb}_2\text{Pt}_2\text{Pb}$. Yb atoms occupy two inequivalent sites with local $m2m$ symmetry, lying at the intersections of the (001), (110), and $(\bar{1}\bar{1}0)$ mirror planes. It is well known that magnetic moments must lie in mirror planes or be perpendicular to

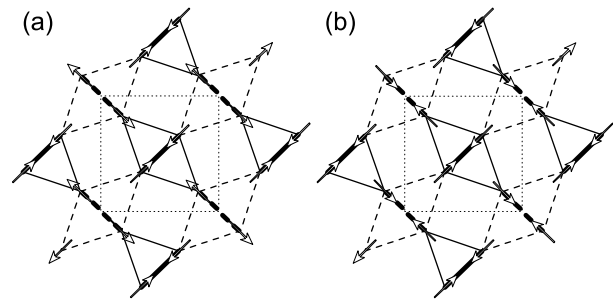


FIG. 7: Schematic representation of an expected magnetic structure on Yb layers. (a) $\text{U}_2\text{Pt}_2\text{Sn}$ type and (b) GdB_4 type.

them. The very low values of $\chi_{[001]}$ and $M_{[001]}$ indicate that the magnetic moments of the Yb^{3+} ions in Yb layers lie in the (001) plane. By analogy to the magnetic structures of $\text{U}_2\text{Pt}_2\text{Sn}$ and GdB_4 ,[32, 33] the Yb moments are probably aligned along $[110]$ and $[\bar{1}\bar{1}0]$, in agreement with the anisotropy between the saturation moments of $M_{[110]}$ and $M_{[\bar{1}\bar{1}0]}$. Two possible magnetic structures which are consistent with these constraints are shown in Fig. 7.

The onset of antiferromagnetic order from a strongly frustrated paramagnetic state, as we observed in $\text{Yb}_2\text{Pt}_2\text{Pb}$, is consistent with theoretical expectations for the Shastry-Sutherland model. The strong magnetic anisotropy confirms that the moments lie in the rare earth layers. In both layer types, the Yb moments lie on a lattice of isosceles triangles ($d_2 < d_1$ and $d_4 < d_3$). This separation of nearest Yb neighbors and next nearest Yb neighbors results in a separation of the antiferromagnetic exchange interactions ($J_1 < J_2$ and $J_3 < J_4$), leading to the formation of well-defined pairs of Yb nearest neighbors in the two rare earth layers (see Fig. 1(b)). In this way, the arrangement of the rare earth ions in both layer types in $\text{Yb}_2\text{Pt}_2\text{Pb}$ are separately equivalent topologically to the lattice of the Shastry-Sutherland model. Accordingly, the magnetic structure inferred from the magnetization measurements (Fig. 7) consists of sheets of orthogonal Yb dimers.

There is considerable evidence for the influence of frustration on the magnetic properties of $\text{Yb}_2\text{Pt}_2\text{Pb}$. A universal feature of magnetically frustrated systems is that magnetic order occurs at temperatures which are much smaller than the scale of the interactions revealed by the Weiss temperatures. By this measure, $\text{Yb}_2\text{Pt}_2\text{Pb}$ is highly frustrated, since the Weiss scale, implies that the mean field interactions are more than two orders of magnitude stronger than the 2.07 K ordering transition. The broad maximum in $\chi_{[100]}$ just above the magnetic ordering temperature is also suggestive of the short range magnetic disorder common to systems with strong magnetic frustration. We have considered the possibility that the Kondo effect is responsible for these departures from ideal local moment behavior. Since it is a single ion phenomenon, manifestations of the Kondo ef-

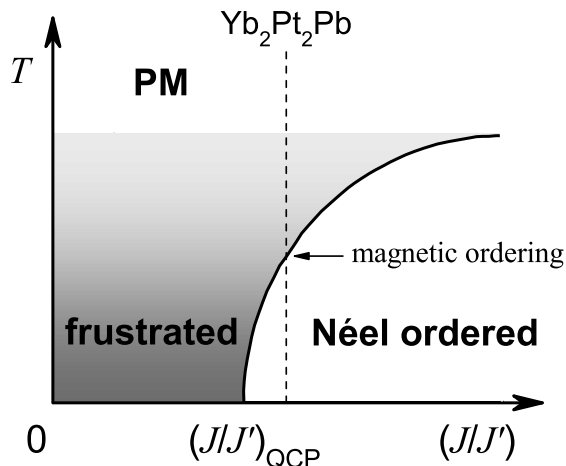


FIG. 8: Schematic phase diagram for the Shastry-Sutherland lattice(see text).

fect should display no significant anisotropy. However, we see that the susceptibility maximum is most pronounced in $\chi_{[100]}$, suggesting that its origin must instead be related to the intrinsic magnetic anisotropy of $\text{Yb}_2\text{Pt}_2\text{Pb}$. In agreement with our results, similar maxima are found in the anisotropic susceptibilities of $\text{SrCu}_2(\text{BO}_3)_2$, TmB_4 and ErB_4 where the magnetic ions also lie on the Shastry-Sutherland network, and where no Kondo effect is likely.[27, 29] We conclude that the broad maximum in $\chi_{[100]}$ reflects excess magnetic fluctuations in the moment bearing planes, originating with the geometrically frustrated Shastry-Sutherland lattice. These fluctuations are also responsible for the slow recovery of the magnetic entropy above the ordering temperature, detected as long tails in the specific heat and electrical resistivity which extend to temperatures as large as ~ 10 K, i.e. five times the transition temperature itself.

The scenario in which long-range antiferromagnetic order emerges from a frustrated magnetic liquid in $\text{Yb}_2\text{Pt}_2\text{Pb}$ is consistent with our expectations of the Shastry-Sutherland lattice. Zero temperature calculations for spin- $\frac{1}{2}$ moments in the two-dimensional Shastry-Sutherland lattice [37] predict a quantum critical point when the ratio of the nearest neighbor J' and next nearest neighbor J exchange interactions $(J/J')_{\text{QCP}}=0.7$. As shown in Fig. 8, the quantum critical point separates a magnetically frustrated spin liquid for $J/J' < (J/J')_{\text{QCP}}$ from a Néel ordered ground state with $J/J' > (J/J')_{\text{QCP}}$. While there is little theoretical guidance regarding the finite temperature properties of the Shastry-Sutherland lattice, further increases of (J/J') beyond $(J/J')_{\text{QCP}}=0.7$ are presumed to stabilize the Néel ordered state at progressively higher temperatures, leading to the phase line depicted qualitatively in

Fig. 8. If the dominant physics is that of the Shastry-Sutherland lattice, we assume that $\text{Yb}_2\text{Pt}_2\text{Pb}$ lies in this limit, where antiferromagnetic order emerges from the spin liquid state. In order to establish this conclusively, we must experimentally rule out other factors such as structural modification, more distant neighbor exchange interactions, and the interlayer exchange itself as possible drivers of magnetic order in $\text{Yb}_2\text{Pt}_2\text{Pb}$.

V. CONCLUSION

We have presented the magnetic, transport, and thermal properties of single crystals of $\text{Yb}_2\text{Pt}_2\text{Pb}$ crystalizing in the tetragonal $\text{U}_2\text{Pt}_2\text{Sn}$ -type structure, a superstructure derived from the tetragonal Mo_2FeB_2 -type structure common to most of the $\text{R}_2\text{T}_2\text{M}$ (R=rare earths; T=transition metals; M=Cd, In, Sn, and Pb). Comparison of the crystal structure with that of other compounds reveals that the radii of the T and M atoms together control the lattice parameters, and hence the overall valence of the Yb ions, which are trivalent in $\text{Yb}_2\text{Pt}_2\text{Pb}$. The crystal structure implies a layered magnetic structure, with the Yb ions contained in two different types of planes. In each, the moments lie on contiguous isosceles triangles, which can be mapped onto the Shastry-Sutherland model. Strong magnetic anisotropy is found at low temperatures with $\chi_{[100]}/\chi_{[001]} \sim 30$, indicating that the magnetic moments of the Yb ions are confined to planes, and likely lie along the $[110]$ and $[1\bar{1}0]$ directions. The magnetic structures implied by the magnetization measurements feature planes of orthogonal Yb dimers which lead to spin liquid ground states in other Shastry-Sutherland lattice systems.

Long range antiferromagnetic order occurs at 2.07 K, emerging from a paramagnetic state which magnetic susceptibility, electrical resistivity, and specific heat measurements find to have substantial short range order and frustration. These experimental findings suggest that $\text{Yb}_2\text{Pt}_2\text{Pb}$ may be a rare example of a Shastry-Sutherland lattice system, although additional experimental work is required to demonstrate this definitively.

Acknowledgments

The authors are grateful to C. Broholm and P. Schiffer for useful discussions and to C. Henderson for assistance with the electron-probe microanalysis, which was performed at the University of Michigan Electron Microbeam Analysis Laboratory (EMAL). Work at the University of Michigan and at Stony Brook University is supported by the National Science Foundation under grant NSF-DMR-0405961.

-
- [1] R. A. Gordon, Y. Ijiri, C. M. Spencer, and F. J. DiSalvo, *J. Alloys Compd.* **224**, 101 (1995).
- [2] P. de V. du Plessis, A. M. Strydom, R. Troć, and L. Menon, *J. Phys.:Condens. Matter* **13**, 8375 (2001).
- [3] D. Kaczorowski, P. Rogl, and K. Hiebl, *Phys. Rev. B* **54**, 9891 (1996).
- [4] M. Giovannini, H. Michor, E. Bauer, G. Hilscher, P. Rogl, and R. Ferro, *J. Alloys Compd.* **280**, 26 (1997).
- [5] A. Doğan, S. Rayprol, and R. Pöttgen, *J. Phys.:Condens. Matter* **19**, 26609 (2007).
- [6] E. Bauer, H. Hilscher, H. Michor, Ch. Paul, Y. Aoki, H. Sato, D. T. Adroja, J-G. Park, P. Bonville, C. Godart, J. Sereni, M. Giovannini, and A. Saccone, *J. Phys.:Condens. Matter* **17**, S999 (2005).
- [7] S. K. Dhar, R. Settai, Y. Ōnuki, A. Gavatanu, Y. Haga, P. Manfrinetti, M. Pani, *J. Magn. Magn. Mater.* **308**, 143 (2007).
- [8] R. Hauser, H. Michor, E. Bauer, G. Hilscher, and D. Kaczorowski, *Physica B* **230-232**, 211 (1997).
- [9] L. Havela, V. Sechovský, P. Svoboda, M. Diviš, H. Nakotte, K. Prokeš, F. R. de Boer, A. Purwanto, R. A. Robinson, A. Seret, J. M. Winand, J. Rebizant, J. C. Spirlet, M. Richter, and Eschrig, *J. Appl. Phys.* **76**, 6214 (1994).
- [10] R. Pöttgen, *Z. Naturforsch.* **49b**, 1525 (1994).
- [11] R. Pöttgen, *Z. Naturforsch.* **49b**, 1309 (1994).
- [12] P. Graveriau, F. Mirambet, B. Chevalier, F. Weill, L. Fournès, D. Laffargue, F. Bourée, and J. Etourneau, *J. Mater. Chem.* **4**, 1893 (1994).
- [13] L. C. J. Pereira, J. M. Winand, F. Wastin, J. Rebizant, J. C. Spirlet, 24^{ièmes} Journées des Actinides, Abstract PB.9, Obergurgl (Austria) (1994).
- [14] F. Hulliger, *J. Alloys Compd.* **232**, 160 (1996).
- [15] R. Pöttgen, P. E. Arpe, C. Felser, D. Kufmann, R. Müllmann, B. D. Mosel, B. Künnen, and G. Kotzyba, *J. Solid State Chem.* **145**, 668 (1999).
- [16] I. R. Fischer, Z. Islam, and P. C. Canfield, *J. Magn. Magn. Mater.* **202**, 1 (1999).
- [17] N. Tsujii, H. Kitō, H. Kitazawa, and G. Kido, *J. Alloys Compd.* **322**, 74 (2001).
- [18] M. Giovannini, E. Bauer, H. Michor, G. Hilscher, A. Galatanu, A. Saccone, and P. Rogl, *Intermetallics* **9**, 481 (2001).
- [19] F. Hulliger, *J. Alloys Compd.* **217**, 164 (1995).
- [20] G. Melnyk, H. C. Kandpal, L. D. Gulay, and W. Tremel, *J. Alloys Compd.* **370**, 217 (2004).
- [21] R. Pöttgen, A. Fugmann, R. Hoffmann, U. Ch. Rodewald, and D. Niepmann, *Z. Naturforsch.* **55b**, 155 (2000).
- [22] T. Muramatsu, T. Kanemasa, E. Bauer, M. Giovannini, T. Kagayama, and K. Shimizu, arXiv:0704.3307 (unpublished).
- [23] B. S. Shastry and B. Sutherland, *Physica B* **108**, 1069 (1981).
- [24] H. Kageyama, K. Yoshimura, R. Stern, N. V. Mushnikov, K. Onizuka, M. Kato, K. Kosuge, C. P. Slichter, T. Goto, and Y. Ueda, *Phys. Rev. Lett.* **82**, 3168 (1999).
- [25] H. Kageyama, K. Onizuka, T. Yamauchi, Y. Ueda, S. Hane, H. Mitamura, T. Goto, K. Yoshimura, and K. Kosuge, *J. Phys. Soc. Jpn.* **68**, 1821 (1999).
- [26] S. Miyahara and K. Ueda, *Phys. Rev. Lett.* **82**, 3701 (1999).
- [27] Z. Fisk, M. B. Maple, D. C. Johnston, and L. D. Woolf, *Solid State Commun.* **39**, 1189 (1981).
- [28] J. Etourneau, J. P. Mercurio, A. Berrada, and P. Hagenmuller, *J. Less-Common Met.* **67**, 531 (1979).
- [29] S. Michimura, A. Shigekawa, F. Iga, M. Sera, T. Takabatake, K. Ohoyama, and Okabe, *Physica B* **378-380**, 596 (2006).
- [30] S. Yoshii, T. Yamamoto, M. Hagiwara, A. Shigekawa, S. Michimura, F. Iga, T. Takabatake, and K. Kindo, *J. Phys.: Conf. Seri.* **51**, 59 (2006).
- [31] F. Iga, A. Shigekawa, Y. Hasegawa, S. Michimura, T. Takabatake, S. Yoshii, T. Yamamoto, M. Hagiwara, K. Kindo, *J. Magn. Magn. Mater.* **310**, e443 (2007).
- [32] K. Prokeš, P. Svoboda, A. Kolomiets, V. Sechovský, H. Nakotte, F. R. de Boer, J. M. Winand, J. Rebizant, and J. C. Spirlet, *J. Magn. Magn. Mater.* **202**, 451 (1999).
- [33] J. A. Blanco, P. J. Brown, A. Stunault, K. Katsumata, F. Iga, and S. Michimura, *Phys. Rev. B* **73**, 212411 (2006).
- [34] M. E. Fisher and J. S. Langer, *Phys. Rev. Lett.* **20**, 665 (1968); S. Alexander, J. S. Helman, and I. Balberg, *Phys. Rev. B* **13**, 304 (1976).
- [35] M. Albrecht and F. Mila, *Europhys. Lett.* **34**, 145 (1996).
- [36] C. H. Chung, J. B. Marston, and S. Sachdev, *Phys. Rev. B* **64**, 134407 (2001).
- [37] A. Isacsson and O. F. Syljuåsen, *Phys. Rev. B* **74**, 026701 (2006).